

Sound fields in a rectangular enclosure under active sound transmission control

S. K. Lau and S. K. Tang^{a)}

Department of Building Services Engineering, The Hong Kong Polytechnic University, Hung Hom, Hong Kong, People's Republic of China

(Received 10 May 2000; revised 24 January 2001; accepted 24 May 2001)

The present study evaluates the effectiveness of active sound transmission control inside an enclosure using a purely acoustic source under the potential energy, squared pressure, and energy density control algorithms. Full coupling between a flexible boundary wall and the interior acoustic cavity is considered. Formulas based on the impedance-mobility approach are developed for the active control of sound transmission with the energy density control algorithm. The resultant total acoustic potential energy attenuation and sound fields under the three control algorithms are compared. Global amplification of the sound level with localized quiet zones under the squared pressure control is observed. This adverse effect can be removed by using the energy density control. It is also shown that the energy density control provides a more uniform control of sound field. Better performance of global and local control of sound field using the squared pressure and energy density controls can be achieved by locating the error sensors at the peak quiet zones and the areas of peak energy density attenuation, respectively, obtained under potential energy control. © 2001 Acoustical Society of America. [DOI: 10.1121/1.1387095]

PACS numbers: 43.50.Ki, 43.55.Rg [MRS]

I. INTRODUCTION

Sound transmission through building fabrics has long been a problem in building noise control. This transmission of noise is mainly due to the interaction between sound fields and the flexible structure boundaries that make up the fabrics or simply a composite wall. However, such flexible structures can hardly be eliminated in reality. For example, in residential buildings, a certain level of window area is necessary for humans both from the physiological and psychological points of view,¹ as well as for providing natural lighting. Inside industrial buildings, windows provide transparency for monitoring purposes. Traditional passive control methods using a double-glazing setup or thicker glass are not usually cost effective, especially for low frequency applications.

Fuller and Jones² proposed the active structural acoustic control method (ASAC) to tackle sound transmission into the fuselage, and showed that it is highly effective to low frequency noise. Pan *et al.*³⁻⁵ extended the analysis of ASAC to the rectangular panel-cavity system using total acoustic potential energy as the performance function. They discovered two modes of ASAC, namely the panel-controlled and cavity-controlled modes. The application of these control modes depends on the relative dominance of the panel structural and cavity modes. Since then, there have been rigorous studies into the use of a point force in ASAC (for instance, Qiu *et al.*⁶). Recently, Cazzolato and Hansen⁷ proposed an error sensing criterion with surface mounted structural vibration sensors for ASAC. It appears that most of the previous studies were focused on using forces applied to the structure

to control the panel-controlled modes. However, most of actuators and sensors for vibration control tend to obstruct the line of sight through windows. This is not desirable for either residential buildings or building services plantrooms. Also, ASAC is effective for suppressing panel modes only, and simply helps to reconstruct the panel velocity distribution in the case of cavity-controlled modes.³ Some disadvantages of ASAC are discussed by Qui *et al.*,⁶ such as the fact that the system requires higher accuracy to produce stable effective global sound attenuation and is not effective if the acoustic energy is transmitted from one structural mode to only one acoustic mode.

In the authors' opinion, the use of acoustic control sources in the active control of sound transmission is worth exploring in order to limit the numbers of vibration actuators and sensors required on critical structures. Snyder and Hansen^{8,9} have considered the use of a hybrid control system with both acoustic and vibration control sources. Kim and Brennan¹⁰ have tested the performance of such a concept in a long enclosure with the impedance and mobility approach. The acoustic control source has been shown to be very effective in controlling cavity-controlled modes inside an enclosed space.^{9,10} Therefore, the effectiveness of acoustic control sources in the active control of sound transmission should not be overlooked.

For the error sensing criteria, the minimization of total acoustic potential energy (potential energy control) is difficult to implement in practice due to the lack of modal sensors. While the traditional error criterion of minimizing the sum of squared sound pressures at discrete locations (squared pressure control) can only provide local control of sound within confined zones of quiet¹¹ due to the limitation of the local information fed to the controller, Joseph *et al.*¹¹ found that the increase in the sound pressure level far from the 10

^{a)} Author to whom correspondence should be addressed; electronic mail: besktang@polyu.edu.hk

dB quiet zone is negligible if the point of cancellation is very close to the secondary source. However, this may not be the case for a nondiffused sound field.¹⁴ In order to cope with a more global control of the enclosed sound field, Sommerfeldt and Nashif¹² and Park and Sommerfeldt¹³ suggested the minimization of the sum of energy densities at discrete locations (energy density control) as the error criterion. Lau and Tang¹⁴ investigated the performance of various error criteria in the active control of indoor noise using acoustic secondary sources. Their results show that better sound fields and zones of quiet inside the enclosure could be achieved with energy density sensing. Sampath and Balachandran¹⁵ also examined the effectiveness of various error functions for ASAC, while Cazzolato¹⁶ and Kim¹⁷ analyzed the resultant total acoustic potential energy of active sound transmission control using vibration and/or acoustic control sources under energy density and squared pressure controls, respectively.

Though the control of sound transmission into a rectangular enclosure is not a new topic, many previous works (for instance, Pan *et al.*,³ Park and Sommerfeldt,¹³ Cazzolato¹⁶ and Kim¹⁷) evaluate the effectiveness of global noise control by using a single parameter of total acoustic potential energy. However, it is possible that the active control may produce an overall reduction of the total potential energy with localized areas of sound amplification. Direct comparison between the performance of different error sensing schemes and forcing methods in three-dimensional enclosed spaces in existing literature is therefore, in the opinion of the authors, incomplete. Also, the performance of error sensing in high energy density attenuation regions obtained under the potential energy control scheme is unknown.

The present study analyzes the sound field and the effectiveness of active sound transmission control with a purely internal acoustic control source under various error sensing schemes. Full couplings between the panel vibration and the room acoustic modes are considered. The existence of amplification and quiet zones and their distributions inside the enclosure are also discussed. Poor performance of active control is expected when the error sensor is located at the nodal plane of the sound field and energy density field for the squared pressure and the energy density control, respectively.¹⁸ The performance of active sound transmission control with various error sensor locations not on the nodal planes is analyzed. It is hoped that a more complete picture of the use of active control in building acoustics can be revealed.

II. OPTIMIZED ACOUSTIC AND VIBRATION CONTROL SOURCE STRENGTHS

A. Potential energy control

Total acoustic potential energy in an enclosed space is widely used as the parameter in assessing the global control effectiveness of an error sensing scheme.^{5,13} This total acoustic potential energy inside an enclosed space of volume V can be written as

$$PE = \frac{1}{4\rho_a c^2} \int_V |p|^2 dV, \quad (1)$$

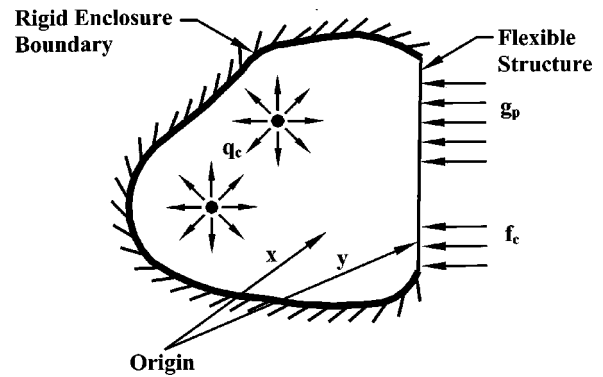


FIG. 1. Structural-acoustic coupled system.

where ρ_a and c are the air density and the speed of sound, and p denotes the complex sound pressure at a point inside the enclosed space. Considering an arbitrary shaped enclosure with a flexible boundary as shown in Fig. 1, \mathbf{x} and \mathbf{y} represent position vectors in the acoustic field inside the enclosure and on the flexible structure, respectively. The primary enclosed sound field (noise field) is due to the external modal force matrix, \mathbf{g}_p , on the flexible boundary. A matrix $\mathbf{t}_c = [\mathbf{f}_c^T \mathbf{q}_c^T]^T$ can be established, where \mathbf{f}_c and \mathbf{q}_c are the column vectors comprised of the strengths of the vibration control forces $[f_{c,1} f_{c,2} \dots]^T$ and acoustic control sources $[q_{c,1} q_{c,2} \dots]^T$ at discrete locations on the flexible boundary and inside the enclosure, respectively. Superscript \mathbf{T} denotes the matrix transpose. The optimized secondary source strengths of the potential energy control for sound transmission are given by Kim¹⁷ as

$$\mathbf{t}_{c,PE} = -\{\mathbf{R}^H \mathbf{Z}_a^H \mathbf{A}^H \mathbf{A} \mathbf{Z}_a \mathbf{R}\}^{-1} \mathbf{R}^H \mathbf{Z}_a^H \mathbf{A}^H \mathbf{A} \mathbf{Z}_a \mathbf{C} \mathbf{Y}_s \mathbf{g}_p, \quad (2)$$

where

$$\mathbf{R} = [\mathbf{C} \mathbf{Y}_s \mathbf{D}_f \quad \mathbf{D}_q] \quad (3)$$

and

$$\mathbf{A} = (\mathbf{I} + \mathbf{Z}_a \mathbf{Y}_{cs})^{-1}. \quad (4)$$

Superscript \mathbf{H} denotes the Hermitian transpose. \mathbf{Z}_a and \mathbf{Y}_s are the uncoupled acoustic modal impedance matrix with N number of acoustic modes and the uncoupled structural modal mobility matrix with M number of structural modes, respectively. \mathbf{C} is a $N \times M$ matrix of the structural-acoustic mode shape coupling coefficient with the elements $C_{n,m}$ as

$$C_{n,m} = \int_{S_f} \psi_n(\mathbf{x}) \phi_m(\mathbf{y}) dS,$$

where S_f denotes the area of the flexible boundary, and $\psi_n(\mathbf{x})$ and $\phi_m(\mathbf{y})$ represent the n th and the m th eigenfunctions of the acoustic and the structural mode distributions, respectively. \mathbf{Y}_{cs} denotes the coupled structural modal mobility matrix ($\mathbf{C} \mathbf{Y}_s \mathbf{C}^T$) and \mathbf{I} unit matrix. \mathbf{D}_q is a $N \times Q$ matrix denoting the couplings between N number of acoustic modes and Q number of acoustic control source locations. \mathbf{D}_f is an $M \times F$ matrix describing the couplings between M number of structural modes and F number of force control actuator locations. The (n,q) and (m,f) elements of \mathbf{D}_q and \mathbf{D}_f are given by

$$D_q(n, q) = \int_V \psi_n(\mathbf{x}) \chi_a(\mathbf{x}_q) dV$$

and

$$D_f(m, f) = \int_{S_f} \phi_m(\mathbf{y}) \chi_f(\mathbf{y}_f) dS,$$

respectively, where $\chi_a(\mathbf{x}_q)$ and $\chi_f(\mathbf{y}_f)$ are the acoustic and vibration source strength distribution functions at \mathbf{x}_q and \mathbf{y}_f , respectively, and are normalized in the rest of this paper by their corresponding $q_{c,d}$ and $f_{c,f}$, respectively. A detailed derivation of Eq. (2) can be found in Kim.¹⁷

B. Squared pressure control

A control scheme that minimizes the sum of the measured squared sound pressures at discrete locations is the most practical and marketable of all those considered in the present study. In this section, the solution of optimal control source strengths for such a control algorithm will be obtained using the impedance and mobility approach.¹⁷ Complex sound pressures at d number of measuring points inside an enclosure can be expressed as

$$\mathbf{p} = \mathbf{\Psi}^H \mathbf{a}, \quad (5)$$

where \mathbf{p} is a column vector of $[p(\mathbf{x}_1, \omega) p(\mathbf{x}_2, \omega) p(\mathbf{x}_3, \omega) \cdots p(\mathbf{x}_d, \omega)]^T$, and $\mathbf{\Psi}$ and \mathbf{a} are the $N \times d$ acoustic mode shape matrix and the $N \times 1$ complex amplitude matrix, respectively. Also, it can be shown that

$$\mathbf{\Psi} = \begin{bmatrix} \psi_1(\mathbf{x}_1) & \psi_1(\mathbf{x}_2) & \cdots & \psi_1(\mathbf{x}_d) \\ \psi_2(\mathbf{x}_1) & \ddots & & \\ \vdots & & \ddots & \\ \psi_N(\mathbf{x}_1) & & & \psi_N(\mathbf{x}_d) \end{bmatrix} \quad (6)$$

and

$$\mathbf{a} = \mathbf{AZ}_a(\mathbf{Rt}_c + \mathbf{CY}_s \mathbf{g}_p). \quad (7)$$

The sum of the squared sound pressures for the measuring points is given as

$$\mathbf{p}^H \mathbf{p} = \mathbf{a}^H \mathbf{\Psi} \mathbf{\Psi}^H \mathbf{a}. \quad (8)$$

A Hermitian quadratic equation is obtained by substituting Eqs. (6) and (7) into Eq. (8), and the optimal secondary source strength matrix that minimizes E number of sound pressure signals can be written as

$$\mathbf{t}_{c,SP} = - \{ \mathbf{R}^H \mathbf{Z}_a^H \mathbf{A}^H \mathbf{\Psi}_e \mathbf{\Psi}_e^H \mathbf{AZ}_a \mathbf{R} \}^{-1} \times \mathbf{R}^H \mathbf{Z}_a^H \mathbf{A}^H \mathbf{\Psi}_e \mathbf{\Psi}_e^H \mathbf{AZ}_a \mathbf{CY}_s \mathbf{g}_p, \quad (9)$$

where $\mathbf{\Psi}_e$ is the acoustic mode shape matrix at the locations of the E number of sound pressure sensors that provide the error signals. Compared with Eq. (2) for the case of the potential energy control, Eq. (9) includes an extra term of error sensing mode shape matrix $\mathbf{\Psi}_e$.

C. Energy density control

As discussed by Lau and Tang,¹⁴ the energy density control is a promising algorithm for both global and local noise control inside an enclosed space. The energy density, ED, at

a measuring point inside an enclosure is the sum of the acoustic potential and the kinetic energy densities:

$$ED = \frac{|p|^2}{2\rho_a c^2} + \frac{\rho_a |u|^2}{2}, \quad (10)$$

where u is the particle velocity at the measuring point. ED provides more global information to the controller, as suggested by Eq. (10). It consists of the local sound pressure and particle velocity, and is less likely to vanish than the sound pressure. Though nodes in the three-dimensional energy density field exist, the nodal volumes for the total energy density field are much smaller than those of the squared pressure field.¹⁸ Using Eq. (5), Eq. (10), and Euler's equation $\nabla p \approx -jk\rho_a c u$, the sum of the energy density at discrete points can be expressed in a matrix form as

$$ED_{\text{sum}} = \frac{1}{2\rho_a c^2} \left\{ \mathbf{p}^H \mathbf{p} + \frac{1}{k^2} \nabla \mathbf{p}^H \cdot \nabla \mathbf{p} \right\}, \quad (11)$$

where k is the wave number. The sensing of energy density signals can be practically achieved by careful arrangement of microphones to measure the acoustic pressures and the three orthogonal components of pressure gradients shown in Eq. (11). The number of pressure microphones required to measure a local energy density can be reduced to four in the tetrahedral configuration.¹⁶ Substituting Eqs. (5) and (7) into Eq. (11), one can find that ED_{sum} for E number of local energy density signals can be expressed as

$$ED_{\text{sum}} = \frac{1}{2\rho_a c^2} J_{ED},$$

where J_{ED} , the cost function of energy density control, is the Hermitian quadratic expression

$$J_{ED} = \mathbf{t}_c^H \mathbf{F}_1 \mathbf{t}_c + \mathbf{F}_2^H \mathbf{t}_c + \mathbf{t}_c^H \mathbf{F}_2 + \mathbf{F}_3$$

with

$$\mathbf{F}_1 = \mathbf{R}^H \mathbf{Z}_a^H \mathbf{A}^H \left[\mathbf{\Psi}_e \mathbf{\Psi}_e^H + \frac{1}{k^2} \nabla \mathbf{\Psi}_e \cdot \nabla \mathbf{\Psi}_e^H \right] \mathbf{AZ}_a \mathbf{R},$$

$$\mathbf{F}_2 = \mathbf{R}^H \mathbf{Z}_a^H \mathbf{A}^H \left[\mathbf{\Psi}_e \mathbf{\Psi}_e^H + \frac{1}{k^2} \nabla \mathbf{\Psi}_e \cdot \nabla \mathbf{\Psi}_e^H \right] \mathbf{AZ}_a \mathbf{CY}_s \mathbf{g}_p,$$

and

$$\mathbf{F}_3 = \mathbf{g}_p^H \mathbf{Y}_s^H \mathbf{C}^H \mathbf{Z}_a^H \mathbf{A}^H \left[\mathbf{\Psi}_e \mathbf{\Psi}_e^H + \frac{1}{k^2} \nabla \mathbf{\Psi}_e \cdot \nabla \mathbf{\Psi}_e^H \right] \mathbf{AZ}_a \mathbf{CY}_s \mathbf{g}_p.$$

The optimal secondary source strengths of energy density control are derived herein by minimizing the resultant Hermitian quadratic expression for J_{ED} . One obtains

$$\mathbf{t}_{c,ED} = - \left\{ \mathbf{R}^H \mathbf{Z}_a^H \mathbf{A}^H \left[\mathbf{\Psi}_e \mathbf{\Psi}_e^H + \frac{1}{k^2} \nabla \mathbf{\Psi}_e \cdot \nabla \mathbf{\Psi}_e^H \right] \mathbf{AZ}_a \mathbf{R} \right\}^{-1} \cdot \mathbf{R}^H \mathbf{Z}_a^H \mathbf{A}^H \left[\mathbf{\Psi}_e \mathbf{\Psi}_e^H + \frac{1}{k^2} \nabla \mathbf{\Psi}_e \cdot \nabla \mathbf{\Psi}_e^H \right] \mathbf{AZ}_a \mathbf{CY}_s \mathbf{g}_p. \quad (12)$$

Equation (12) consists of an additional matrix of $(\mathbf{\Psi}_e \mathbf{\Psi}_e^H + \nabla \mathbf{\Psi}_e \cdot \nabla \mathbf{\Psi}_e^H / k^2)$, which consists of the normalized total energy density fields at the locations of the E number of energy

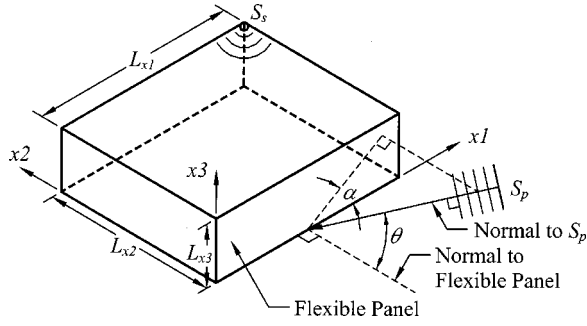


FIG. 2. Rectangular enclosed space and coordinate system.

density sensors that provide the error signals, compared with Eq. (2) for the potential energy control.

III. NUMERICAL MODEL AND COMPUTATIONAL CONVERGENCE

A numerical experiment was performed to evaluate the performance of various error sensing criteria for the active control of sound transmission. Figure 2 illustrates the rectangular enclosure and the coordinate system adopted in the present study. The dimensions of the enclosure are L_{x1} (length), L_{x2} (width), and L_{x3} (height) which were chosen such that $L_{x1}:L_{x2}:L_{x3}=1:e/\pi:1/\pi$ so as to avoid the degenerate acoustic modes.¹⁹ The enclosure consists of five acoustically rigid walls and a simple supported flexible panel at $x_2=0$. The primary enclosed sound fields are due to the interaction between the interior acoustic space and the structural vibration on the flexible panel excited by an external plane wave S_p of frequency ω . The propagation direction of S_p is defined by the incidence angle θ and azimuth α as shown in Fig. 2. The incidence angle θ is defined as the angle between the lines normal to the external plane wave and the flexible panel, while the azimuth α is the angle between the projected plane of the line normal to the external plane wave on the panel and the x_1 axis. In the present investigation, the secondary acoustic control source, S_s , is located at the corner (L_{x1}, L_{x2}, L_{x3}) in order to avoid the nodal lines of any acoustic mode in the rectangular enclosure.^{14,20} Two new dimensionless parameters, η_c and φ , are introduced herein as

$$\eta_c = \frac{K_a}{M_s \omega_{ac} \omega_{sc}}, \quad (13)$$

and

$$\varphi = \frac{\omega_{ac}}{\omega_{sc}} = \sqrt{\frac{\rho_s h}{D}} \left(\frac{1}{L_{y1}^2} + \frac{1}{L_{y2}^2} \right)^{-1} \frac{c}{\pi L_{x,\max}}, \quad (14)$$

respectively, where K_a and M_s are the acoustic bulk stiffness ($\rho_a c^2 S_f^2/V$) and mass of the structure ($\rho_s h S_f$), respectively, and ω_{ac} and ω_{sc} are the first eigenfrequencies of acoustic (cavity) and structural (panel) modes, respectively. D , ρ_s , S_f , and h are the bending stiffness, density, surface area and thickness of the flexible panel, respectively. $L_{x,\max}$ is the maximum perpendicular separation between two parallel walls inside the rectangular enclosure, and $L_{y1} \times L_{y2}$ are the dimensions of the flexible panel. In the present numerical model, $L_{x,\max} = L_{y1} = L_{x1}$ and $L_{y2} = L_{x3}$. Table I shows some

TABLE I. Possible values of η_c and φ .^a

Flexible structure	L_{x1} (m)	η_c	φ
6 mm glass (Ref. 21)	1	0.01	1.04
6 mm glass (Ref. 21)	5	0.26	5.21
12 mm glass (Ref. 21)	5	0.06	2.60
6 mm alumina (Al_2O_3) (Ref. 21)	5	0.10	3.05
Kim and Brennan (Refs. 10 and 22)	1.5	0.04	0.81

^aAir density and speed of sound in air 20 °C are 1.21 kg/m³ and 340 m/s, respectively.

possible values of η_c and φ . Then, Eqs. (3), (4), and (7) can be rearranged as follows:

$$\mathbf{a} = \eta_c \mathbf{A} \hat{\mathbf{Z}}_a (\hat{\mathbf{R}} \hat{\mathbf{t}}_c + \hat{\mathbf{C}} \hat{\mathbf{Y}}_s \hat{\mathbf{g}}_p), \quad (15)$$

$$\mathbf{A} = (\mathbf{I} + \eta_c \hat{\mathbf{Z}}_a \hat{\mathbf{Y}}_s)^{-1}, \quad (16)$$

and

$$\hat{\mathbf{R}} = [\hat{\mathbf{C}} \hat{\mathbf{Y}}_s \mathbf{D}_f \quad \mathbf{D}_q], \quad (17)$$

respectively, where $\hat{\mathbf{C}} = \mathbf{C}/S_f$, $\hat{\mathbf{g}}_p = \mathbf{g}_p/S_f$, and $\hat{\mathbf{Y}}_s = \hat{\mathbf{C}} \hat{\mathbf{Y}}_s \hat{\mathbf{C}}^T$. All the above variables are dimensionless except $\hat{\mathbf{g}}_p$ and $\hat{\mathbf{t}}_c$, whose units are Nm⁻². $\hat{\mathbf{Z}}_a$ and $\hat{\mathbf{Y}}_s$ are $(N \times N)$ and $(M \times M)$ diagonal matrices which equal $\{\omega_{ac} V / (\rho_a c^2)\} \mathbf{Z}_a$ and $(\omega_{sc} \rho_s h S_f) \mathbf{Y}_s$, respectively. The (n,n) and (m,m) diagonal elements of $\hat{\mathbf{Z}}_a$ and $\hat{\mathbf{Y}}_s$ consist, respectively, of $\hat{Z}_{a,n}$ and $\hat{Y}_{s,m}$ where

$$\hat{Z}_{a,n} = \frac{j \hat{\omega}}{\hat{\omega}_n^2 - \hat{\omega}^2 + 2j \xi_n \hat{\omega}_n \hat{\omega}}, \quad (18)$$

$$\hat{Y}_{s,m} = \frac{j \hat{\omega} \varphi}{\hat{\omega}_m^2 - \hat{\omega}^2 \varphi^2 + 2j \zeta_m \hat{\omega}_m \hat{\omega} \varphi}, \quad (19)$$

and $\hat{\omega}$ is the normalized angular frequency (normalized by ω_{ac}). $\hat{\omega}_n$ and $\hat{\omega}_m$ are the acoustic and structural mode frequencies normalized by their first eigenfrequencies, respectively (ω_{ac} and ω_{sc} , respectively). ξ_n and ζ_m are the modal damping coefficients of the acoustic and structural modes, respectively. The secondary source strength matrix can be rewritten as

$$\hat{\mathbf{t}}_c = \begin{bmatrix} \hat{\mathbf{t}}_c \\ \hat{\mathbf{q}}_c \end{bmatrix}, \quad (20)$$

where $\hat{\mathbf{t}}_c = \mathbf{t}_c/S_f$ and $\hat{\mathbf{q}}_c = \mathbf{q}_c/(\omega_{sc} \rho_s h/S_f)$. Comparing the expression for $\hat{\mathbf{q}}_c$ and $\hat{\mathbf{g}}_p$, it can be noted that a weaker secondary acoustic control source is required to control a fixed external primary sound source under higher ω_{sc} and/or panel surface density, $\rho_s h$.

Equations (2), (9), and (12) for the optimal secondary source strength matrix can now be rewritten using the non-dimensional parameters:

$$\hat{\mathbf{t}}_{c,PE} = -\{\hat{\mathbf{R}}^H \hat{\mathbf{Z}}_a^H \mathbf{A}^H \hat{\mathbf{Z}}_a \hat{\mathbf{R}}\}^{-1} \hat{\mathbf{R}}^H \hat{\mathbf{Z}}_a^H \mathbf{A}^H \hat{\mathbf{Z}}_a \hat{\mathbf{C}} \hat{\mathbf{Y}}_s \hat{\mathbf{g}}_p, \quad (21)$$

$$\hat{\mathbf{t}}_{c,SP} = -\{\hat{\mathbf{R}}^H \hat{\mathbf{Z}}_a^H \mathbf{A}^H \Psi_e \Psi_e^H \mathbf{A} \hat{\mathbf{Z}}_a \hat{\mathbf{R}}\}^{-1} \times \hat{\mathbf{R}}^H \hat{\mathbf{Z}}_a^H \mathbf{A}^H \Psi_e \Psi_e^H \mathbf{A} \hat{\mathbf{Z}}_a \hat{\mathbf{C}} \hat{\mathbf{Y}}_s \hat{\mathbf{g}}_p, \quad (22)$$

$$\hat{\mathbf{t}}_{c,ED} = - \left\{ \hat{\mathbf{R}}^H \hat{\mathbf{Z}}_a^H \mathbf{A}^H \left[\Psi_e \Psi_e^H + \frac{1}{k^2} \nabla \Psi_e \cdot \nabla \Psi_e^H \right] \mathbf{A} \hat{\mathbf{Z}}_a \hat{\mathbf{R}} \right\}^{-1} \\ \times \hat{\mathbf{R}}^H \hat{\mathbf{Z}}_a^H \mathbf{A}^H \left[\Psi_e \Psi_e^H + \frac{1}{k^2} \nabla \Psi_e \cdot \nabla \Psi_e^H \right] \mathbf{A} \hat{\mathbf{Z}}_a \hat{\mathbf{C}} \hat{\mathbf{Y}}_s \hat{\mathbf{g}}_p. \quad (23)$$

In the foregoing discussions, suffices PE, SP, and ED denote quantities associated with the potential energy, squared pressure, and energy density control algorithms, respectively. $[\Psi_e \Psi_e^H]$ and $[\Psi_e \Psi_e^H + \nabla \Psi_e \cdot \nabla \Psi_e^H / k^2]$ in Eqs. (22) and (23) govern the performance of the squared pressure and energy density controls. They depend directly on the error sensor locations. Parkins *et al.*¹⁸ have investigated these two terms using node structures. As mentioned previously, the energy density control has the advantage of the lower probability of a randomly placed sensor being laid in a nodal volume for acoustic modes, and requiring much fewer sensors than the squared pressure control.

It can be seen from Eq. (15) that the effectiveness of passive sound transmission control depends on the structural-acoustic coupling transfer function (described by \mathbf{A}) and the effectiveness of the vibration force to acoustic pressure transfer function at weak structural-acoustic coupling (represented by $\eta_c \hat{\mathbf{Z}}_a \hat{\mathbf{C}} \hat{\mathbf{Y}}_s$). The two parameters, η_c and φ , are critical for passive sound transmission control. The speed of sound and the air density are practically constant. Thus, the traditional measure for controlling sound transmission is to reduce K_a / M_s in η_c , so that both the magnitudes of the structural-acoustic coupling transfer function and the vibration force to acoustic pressure transfer function at weak structural-acoustic coupling are reduced. Also, some reduction of sound transmission can be achieved by reducing both ω_{ac} and ω_{sc} [Eq. (15)]. Modification of the passive sound transmission control is possible by adjusting φ . However, the eigenfrequency of the flexible panel should not be near to the eigenfrequencies of the enclosure and/or the forcing frequency ω .

Using Eqs. (5), (15), (21), (22), and (23), the attenuation of sound pressure at a point inside the enclosure under the three sound transmission control algorithms can be expressed as

$$\Delta SP = \Psi^H \{ \eta_c \mathbf{A} \hat{\mathbf{Z}}_a \hat{\mathbf{R}} \{ \hat{\mathbf{R}}^H \hat{\mathbf{Z}}_a^H \mathbf{A}^H \mathbf{E} \mathbf{A} \hat{\mathbf{Z}}_a \hat{\mathbf{R}} \}^{-1} \\ \times \hat{\mathbf{R}}^H \hat{\mathbf{Z}}_a^H \mathbf{A}^H \mathbf{E} \mathbf{A} \hat{\mathbf{Z}}_a \hat{\mathbf{C}} \hat{\mathbf{Y}}_s \hat{\mathbf{g}}_p \},$$

where \mathbf{E} is \mathbf{I} , $\Psi_e \Psi_e^H$, and $\Psi_e \Psi_e^H + k^{-2} \nabla \Psi_e \cdot \nabla \Psi_e^H$ for the potential energy, the squared pressure, and the energy density controls, respectively. Besides the terms for passive control, it can be shown that the effectiveness of the active sound transmission control relies on the matrix

$$\hat{\mathbf{R}} \{ \hat{\mathbf{R}}^H \hat{\mathbf{Z}}_a^H \mathbf{A}^H \mathbf{E} \mathbf{A} \hat{\mathbf{Z}}_a \hat{\mathbf{R}} \}^{-1} \hat{\mathbf{R}}^H \hat{\mathbf{Z}}_a^H \mathbf{A}^H \mathbf{E} \mathbf{A} \hat{\mathbf{Z}}_a, \quad (24)$$

which is governed by the source frequency ω , the degree of structural-acoustic coupling, the modal characteristics of the enclosure and the flexible panel, and the error sensing matrix. Kim¹⁷ has investigated the performance of active sound transmission control in a weakly coupled ductlike rectangular enclosure with potential energy control. For such a sys-

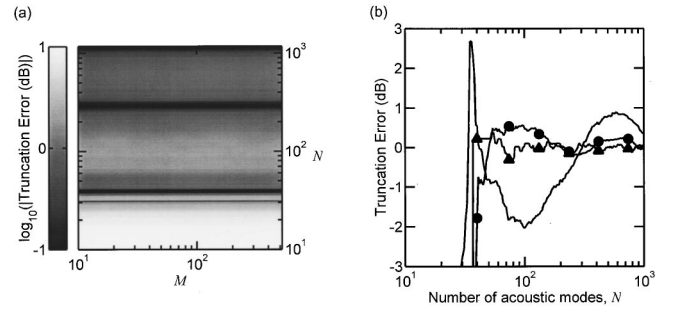


FIG. 3. Convergence of modal summation with point acoustic source at (L_{x1}, L_{x2}, L_{x3}) and forcing frequency $5\omega_{ac}$, $\eta_c = 0.0092$ and $\varphi = 9.2$. (a) At location $(0.9L_{x1}, 0.9L_{x2}, 0.9L_{x3})$ with $N < 1173$ and $M < 522$; (b) effect of location ($M = 522$). — $(0.9L_{x1}, 0.9L_{x2}, 0.9L_{x3})$; —●— $(0.8L_{x1}, 0.8L_{x2}, 0.8L_{x3})$; —▲— $(0.5L_{x1}, 0.5L_{x2}, 0.5L_{x3})$.

tem, $\mathbf{A} \approx \mathbf{I}$ as $\eta_c \hat{\mathbf{Z}}_a \hat{\mathbf{Y}}_{cs} = 0$. This is consistent with the discussions of Kim and Brennan,²² who stated the problem in a different way. Expression (24) becomes independent of η_c for weakly coupled systems. In this paper, fully structural-acoustic coupled systems are discussed with consideration of η_c and φ under three control algorithms, namely the potential energy, squared pressure, and energy density controls.

Though an exact representation of the sound field is given by Eq. (5) with the summation of the contributions from infinite numbers of acoustic and structural modes ($N \rightarrow \infty$ and $M \rightarrow \infty$, respectively), truncating these summations with a finite number of modes in the calculations is reasonably accurate in the estimation of the sound field at low modal densities in practice. Therefore, a convergence test has to be done in the first place to determine the acceptable values for N and M . Equation (5) has an inherent convergence difficulty at locations close to a point acoustic source,²³ but it is not worth studying the sound pressure at these points. The acoustic modal impedance and the structural modal mobility in Eqs. (18) and (19) were obtained with both the acoustic and structural modal damping coefficients of 0.01 in the present study. All the simulations were computed by using MATLAB on a DEC workstation 600 a.u.

Figure 3(a) illustrates the convergence of the near field sound pressure calculated by Eq. (5) at the location $(0.9L_{x1}, 0.9L_{x2}, 0.9L_{x3})$ inside the enclosure shown in Fig. 2 with $\eta_c = 0.0092$, $\varphi = 9.2$ and an acoustic corner source located at (L_{x1}, L_{x2}, L_{x3}) operating at $5\omega_{ac}$. Defining truncation error as the difference between calculated result and that obtained with $N = 1173$ and $M = 522$, it is observed that there is a gradual reduction of such error for $N > 37$. The maximum deviation from the result obtained with $N = 1173$ and $M = 522$ is less than 0.86 dB for $N > 600$, regardless of the number of structural modes involved. Faster convergence can be found at increased distance away from the corner sound source for $N > 37$ in Fig. 3(b).

Figure 4(a) shows the convergence of sound pressure at the center of the enclosure due to an excitation from a point force acting at the center of the flexible panel. A sharp fall of truncation error is revealed for $N > 37$ and $M > 110$. The maximum deviation from the result obtained with $N = 1173$ and $M = 522$ is less than 0.97 dB for $N > 600$ and $M > 110$. Similar and even better convergence can be found at other

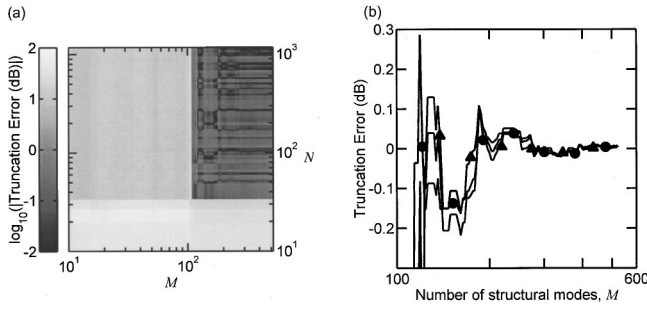


FIG. 4. Convergence of modal summation with point force actuator at $(0.5L_{y1}, 0.5L_{y2})$ and forcing frequency $5\omega_{ac}$, $\eta_c = 0.0092$ and $\varphi = 9.2$. (a) At center of enclosure $(0.5L_{x1}, 0.5L_{x2}, 0.5L_{x3})$; (b) effect of location ($N = 1173$). — $(0.5L_{x1}, 0.5L_{x2}, 0.5L_{x3})$; —●— $(0.9L_{x1}, 0.9L_{x2}, 0.9L_{x3})$; —▲— $(0.5L_{x1}, 0, 0.5L_{x3})$.

points inside the enclosure, as shown in Fig. 4(b). The same phenomenon is observed when the excitation is due to a plane acoustic external source (not shown here). The convergence test has been extended to cover the range $0.0092 \leq \eta_c \leq 0.92$ and $0.092 \leq \varphi \leq 9.2$. Similar or faster computational convergence as in Figs. 3 and 4 can be observed (not shown here). Thus 1173 and 522 numbers of acoustic and structural modes, respectively, were adopted in the present calculations with the consideration of computer power and accuracy. Compared with the details of Kim and Brennan,¹⁰ the present investigation has included far more acoustic and structural modes in the calculations. Also, faster convergence can be achieved for $\omega < 5\omega_{ac}$.

IV. TOTAL ACOUSTIC POTENTIAL ENERGY

A. Effects of η_c and φ under potential energy control

The effectiveness of passive sound transmission control depends mainly on the acoustic bulk stiffness and the mass of the structure, K_a/M_s ,²² which is related to η_c . However, for passive control of sound transmission, the principles of using lighter structures and smaller η_c are contradictory. The application of active sound transmission control will allow the use of lighter structures and/or even further reduce sound pressures inside the enclosure. As mentioned previously, a common metric for assessing the global control effectiveness inside an enclosure is the reduction of the total acoustic potential energy, PE. For orthogonal modal characteristic functions, the integration of potential energy [Eq. (1)] gives

$$PE = \frac{V}{4\rho c^2} \mathbf{a}^H \mathbf{a}. \quad (25)$$

Figure 5 shows the potential energy at frequency $0.2\omega_{ac}$, ω_{ac} , $2.4\omega_{ac}$, and $3\omega_{ac}$ under different combinations of η_c and φ , which are logarithmically distributed into 24×26 divisions between 0.0092 and 0.92 and between 0.092 and 9.2, respectively. The external modal force matrix, $\hat{\mathbf{g}}_p$, results from an external plane wave of unity strength at $\theta = \pi/6$ and $\alpha = \pi/4$. There is, in general, a gradual decline of PE as η_c decreases for all frequencies. This is consistent with the deduction from the passive sound transmission control. Peak PE occurs at $\omega = \omega_{sc}$ for a weakly coupled system. As η_c increases, the peak PE occurs at lower frequency, especially

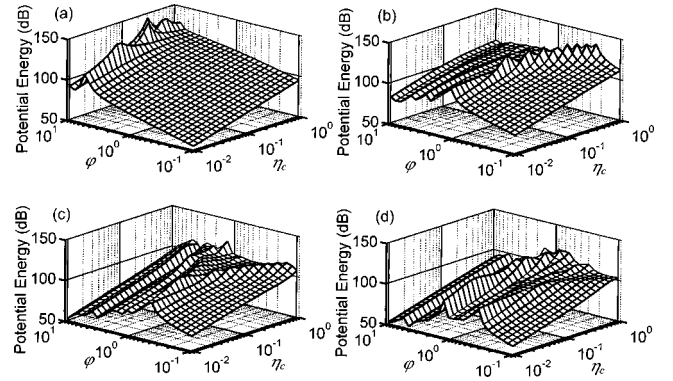


FIG. 5. Variation of total acoustic potential energy with η_c and φ at different forcing frequencies. (a) $0.2\omega_{ac}$; (b) ω_{ac} ; (c) $2.4\omega_{ac}$; (d) $3\omega_{ac}$. Primary external plane source at $\theta = \pi/6$ and $\alpha = \pi/4$. All data presented are in dB ref 10^{-12} Nm.

for a strongly coupled system (where η_c is large). The shift of the PE is due to the effect of the coupling matrix \mathbf{A} in Eq. (15). Such peak PE can be attenuated effectively by active means under the potential energy control using an acoustic control source at (L_{x1}, L_{x2}, L_{x3}) and a force control actuator at the center of the flexible panel, as shown in Fig. 6. Peak PE attenuations usually occur around the η_c and φ combinations that produce high PE at $\omega = \omega_{sc}$ (cf. Fig. 5). Relatively sharp reduction of the PE attenuation is observed at forcing frequency $\omega > \omega_{sc}$ for a weakly coupled system (small η_c), implying that this hybrid active sound transmission control of the global sound field is ineffective at frequencies higher than ω_{sc} when η_c is small. However, a certain degree of the PE attenuation can still be observed at frequency $\omega > \omega_{sc}$ if $\omega < \omega_{ac}$ [Figs. 6(a) and (b)] at the eigenfrequencies of the flexible panel. Also, the frequency at which this sharp fall of PE attenuation occurs is lower than ω_{sc} for a strongly coupled system (large η_c). A plateau of high PE attenuation can also be observed for small φ at $\omega < \omega_{sc}$.

Figures 7 and 8 illustrate the attenuation of PE under the potential energy control with a pure active force actuator at the center of the flexible panel and a pure acoustic control source at (L_{x1}, L_{x2}, L_{x3}) , respectively, at frequency $0.2\omega_{ac}$, ω_{ac} , $2.4\omega_{ac}$, and $3\omega_{ac}$. Active vibration control produces

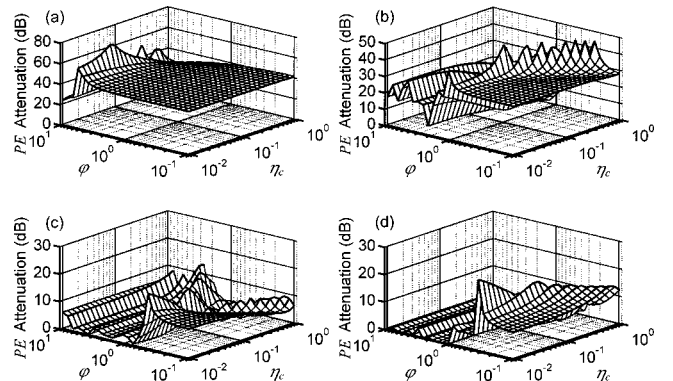


FIG. 6. Variation of total acoustic potential energy attenuation with η_c and φ under potential energy control using hybrid control system at different forcing frequencies. (a) $0.2\omega_{ac}$; (b) ω_{ac} ; (c) $2.4\omega_{ac}$; (d) $3\omega_{ac}$. Primary external plane source at $\theta = \pi/6$ and $\alpha = \pi/4$; acoustic control source at (L_{x1}, L_{x2}, L_{x3}) ; force actuator at $(0.5L_{x1}, 0.5L_{x3})$.

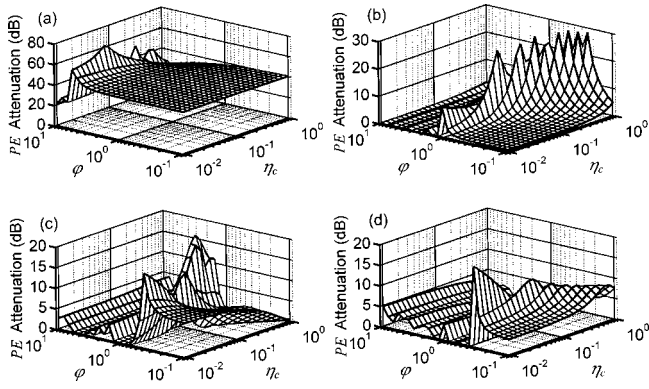


FIG. 7. Variation of total acoustic potential energy attenuation with η_c and φ under potential energy control using purely vibration control at $(0.5L_{x1}, 0.5L_{x3})$ at different forcing frequencies. (a) $0.2\omega_{ac}$; (b) ω_{ac} ; (c) $2.4\omega_{ac}$; (d) $3\omega_{ac}$. Primary external plane source at $\theta = \pi/6$ and $\alpha = \pi/4$.

similar results as those under the hybrid control (Fig. 6). However, the high PE attenuation observed at $\omega = 0.2\omega_{ac}$ falls rapidly as ω increases towards ω_{ac} . The control only becomes effective at the eigenfrequencies of the flexible panel in the cavity-controlled modes when $\omega = \omega_{ac}$, as shown in Fig. 7(b). For pure acoustic control (Fig. 8), high attenuation of PE can also be found at frequency $\omega > \omega_{sc}$ besides the plateau of PE attenuation at smaller η_c and φ pairs for $\omega \leq \omega_{ac}$. The acoustic control source is less effective to control the panel-controlled modes at ω_{sc} near to $\varphi = 5$ and $\varphi = 1$ as shown in Figs. 8(a) and (b), respectively. Only slight attenuation of PE can be found at higher frequencies [Figs. 8(c) and (d)]. Therefore, the pure acoustic control source is effective at frequencies less than ω_{ac} except at ω_{sc} . Comparing the results shown in Figs. 6–8, it is found that the pure acoustic control can provide reasonable acoustic potential energy attenuation in the practical range of φ and η_c (Table I), especially at low forcing frequency, despite its simplicity of construction. This better performance of the pure acoustic control is anticipated, as the higher structural modes of a weak panel structure are poorly excited by a plane wave as a result of modal filtering. However, this plane wave excitation is common in practical building noise transmission problems. A typical example of it is the noise emitted by a distant source transmitted into a room through the weak

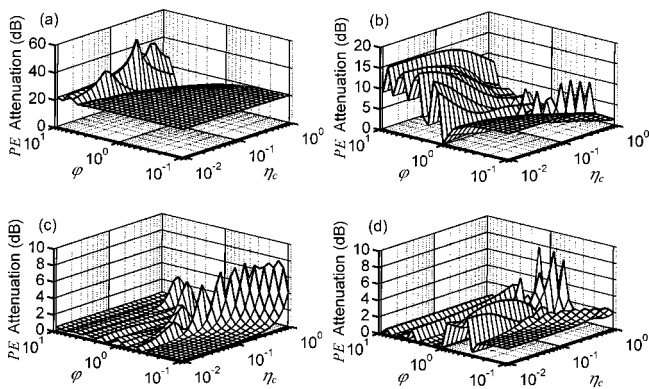


FIG. 8. Variation of total acoustic potential energy attenuation with η_c and φ under potential energy control using purely acoustic control source at (L_{x1}, L_{x2}, L_{x3}) at different forcing frequencies. (a) $0.2\omega_{ac}$; (b) ω_{ac} ; (c) $2.4\omega_{ac}$; (d) $3\omega_{ac}$. Primary external plane source at $\theta = \pi/6$ and $\alpha = \pi/4$.

structures of building fabrics. Therefore, only this control is investigated in the rest of the paper.

B. Total potential energy under different control algorithms

Using the same external plane wave and the acoustic control source configuration as shown in Fig. 2, a single sensor was placed in five discrete locations within the enclosure for five control simulations. These five locations were equally spaced along a diagonal line between the points $(0.9L_{x1}, 0.9L_{x2}, 0.9L_{x3})$ and $(0.1L_{x1}, 0.1L_{x2}, 0.9L_{x3})$ close to the ceiling. At least four control channels are required for measuring the three orthogonal particle velocities and one sound pressure during each energy density sensing. Detailed comparisons between energy density error sensor and four microphones sensing can be found in Cazzolato.¹⁶ Global control is then expected to be poorer for single squared pressure sensing than for energy density sensing. However, for a compact configuration of error sensing devices required in practice, the four microphone squared pressure signals are similar, especially in the practical frequency range of building noise control. Thus, the single microphone for squared pressure control is studied here for simplicity. Figures 9 and 10 show the attenuation of PE up to $5\omega_{ac}$ for each sensor location with $\eta_c = 0.01$, $\varphi = 1.04$ and $\eta_c = 0.26$, $\varphi = 5.21$, respectively. These combinations of η_c and φ correspond to data shown in the first and second rows of Table I for a small box and a room, respectively, with a 6 mm glass panel as the transmitting wall. The calculations were done at $0.02\omega_{ac}$ intervals. Also, attenuation greater than 40 dB and amplification higher than 30 dB were truncated.

It can be observed from Fig. 9 that the attenuation of total potential energy under the potential energy control scheme is high when the frequency of the external sound wave is less than ω_{ac} . Peak attenuation of PE also occurs at some eigenfrequencies, such as $1.16\omega_{ac}$, $1.53\omega_{ac}$, and $2.52\omega_{ac}$, which correspond to the $(0,1,0)$, $(1,1,0)$, and $(1,2,0)$ acoustic modes, respectively. As the frequency increases beyond $3\omega_{ac}$, the attenuation of PE is poor.

The squared pressure control at the above error sensor locations gives a basically similar PE attenuation trend as the potential energy control, but significant amplifications are observed at some frequencies. The ineffective PE attenuation at $1.53\omega_{ac}$ [the $(1,1,0)$ acoustic mode] shown in Fig. 9(c) is due to the location of the error sensor being on two nodal planes (the middle point of the ceiling). Besides the spill-overs at some eigenfrequencies, the detrimental effects of the squared pressure control at frequencies between the room modes occur when the error sensor is located near to the region where the acoustic modes due to the secondary source are destructively interfering with each other. These effects are commonly found and are more significant for near field error sensing strategies at frequencies below ω_{ac} . Typical examples are the large PE amplifications at the frequencies $0.3\omega_{ac}$, $0.6\omega_{ac}$, and ω_{ac} shown in Figs. 9(a), (b), and (c), respectively. The first detrimental effect occurs at lower frequency when the error sensor gets closer to the secondary corner source.¹⁴ The detrimental effects become less significant or can be eliminated when the error sensor is located

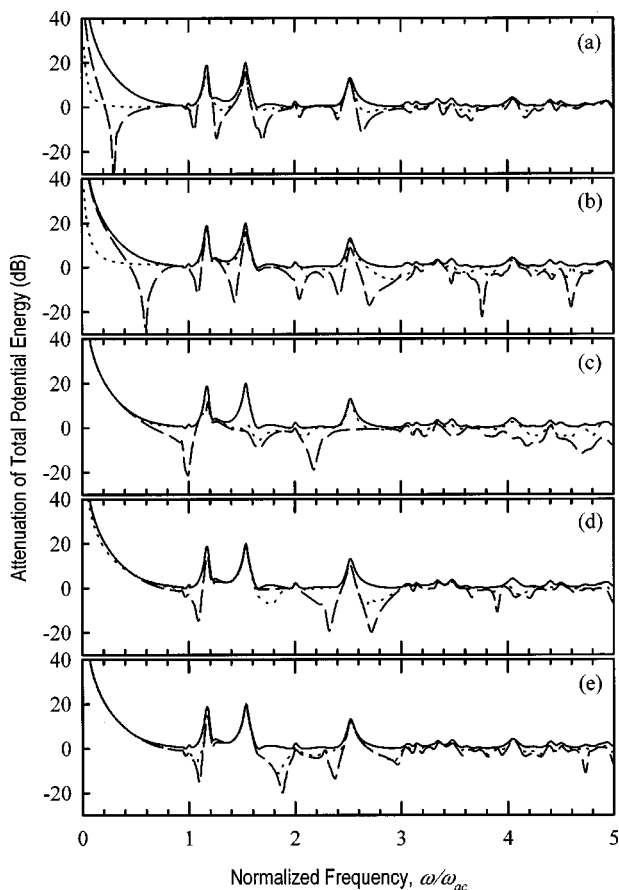


FIG. 9. Variation of total acoustic potential energy attenuation with frequency for primary acoustic source at $\theta = \pi/6$, $\alpha = \pi/4$ under various error sensor locations. (a) $(0.9L_{x1}, 0.9L_{x2}, 0.9L_{x3})$; (b) $(0.7L_{x1}, 0.7L_{x2}, 0.9L_{x3})$; (c) $(0.5L_{x1}, 0.5L_{x2}, 0.9L_{x3})$; (d) $(0.3L_{x1}, 0.3L_{x2}, 0.9L_{x3})$; (e) $(0.1L_{x1}, 0.1L_{x2}, 0.9L_{x3})$. — Potential energy control; ---- squared pressure control; energy density control. Secondary source at (L_{x1}, L_{x2}, L_{x3}) ; $\eta_c = 0.01$ and $\varphi = 1.04$.

near to the corner opposite the secondary source due to the absence of destructively modal interference, as shown in Figs. 9(d) and (e), especially for frequency below ω_{ac} .¹⁴

The use of energy density as the cost function has the advantage of avoiding both detrimental effects and spillovers as suggested in Fig. 9, especially at frequencies below ω_{ac} for all error sensor locations investigated. This is expected, as the energy density control system is more heavily constrained. The particle velocities normal to the acoustically rigid walls of the enclosure vanish, and thus the particle velocities in the three orthogonal directions are zero at a corner of the rectangular enclosure. It can also be observed that the performance of the energy density control algorithm becomes closer to that of the squared pressure one as the error sensor is located towards the corner opposite to the secondary source [Figs. 9(d) and (e)], which is consistent with existing literature, for example, Cazzolato.¹⁶ However, the energy density control becomes ineffective when the error sensor is placed closer to the secondary acoustic control source, due to the nonuniform energy density field produced solely by the secondary source, resulting in a small secondary source strength as shown by Lau and Tang¹⁴ [Figs. 9(a) and (b)].

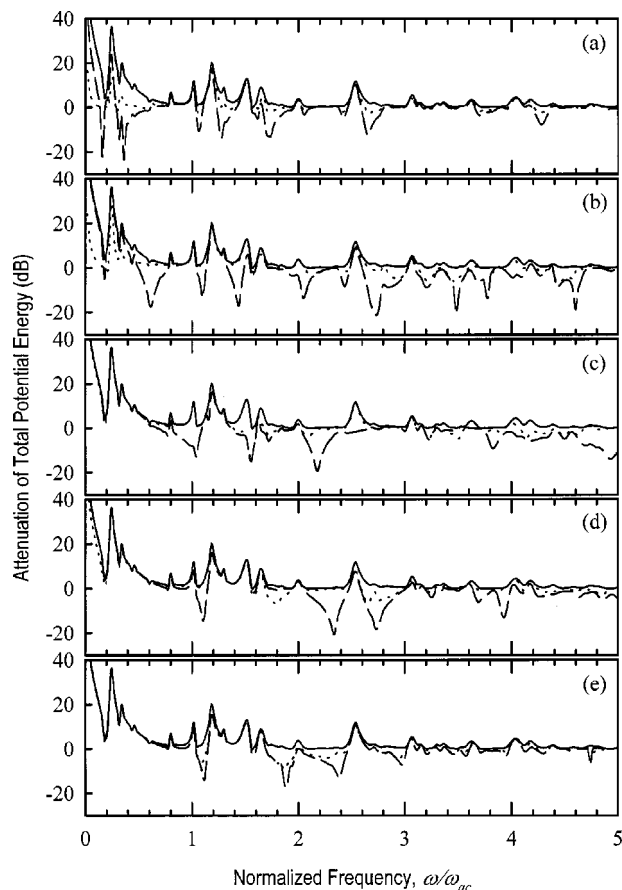


FIG. 10. Variation of total acoustic potential energy attenuation with frequency for primary acoustic source at $\theta = \pi/6$, $\alpha = \pi/4$ under various error sensor locations. (a) $(0.9L_{x1}, 0.9L_{x2}, 0.9L_{x3})$; (b) $(0.7L_{x1}, 0.7L_{x2}, 0.9L_{x3})$; (c) $(0.5L_{x1}, 0.5L_{x2}, 0.9L_{x3})$; (d) $(0.3L_{x1}, 0.3L_{x2}, 0.9L_{x3})$; (e) $(0.1L_{x1}, 0.1L_{x2}, 0.9L_{x3})$. Secondary source at (L_{x1}, L_{x2}, L_{x3}) ; $\eta_c = 0.26$ and $\varphi = 5.21$. Legends are the same as those in Fig. 9.

Basically similar results can be found for larger η_c ($=0.26$) and φ ($=5.21$) (that is, stronger acoustic-panel coupling), as shown in Fig. 10. However, the PE at frequencies near to $0.19\omega_{ac}$ ($=\omega_{sc}$) is not effectively attenuated by all the three control algorithms even though they are far below ω_{ac} and the associated secondary acoustic source strength is high [Fig. 11(a)]. This is because of the ineffective generation of PE by the secondary acoustic source at ω_{sc} , as shown in Fig. 11(b), especially for $\omega_{sc} \ll \omega_{ac}$. Additional detrimental effects at frequency $0.16\omega_{ac}$ are observed for the squared pressure control as shown in Fig. 10(a) [cf. Fig. 9(a)], suggesting that near field error sensing is not suitable for the squared pressure control under strong acoustic-panel coupling.

It can be seen from Figs. 9 and 10 that the attenuation of PE becomes insignificant at frequencies higher than $3\omega_{ac}$ for all the three control algorithms discussed, while that under the squared pressure control shows the tendency of amplification. However, the coexistence of “quiet zones” and “amplification zones” is possible within an enclosure under the active control. Sometimes, a large global increase of the sound pressure level may occur when the quiet zones are improperly forced by the control scheme. Also, the sound field inside an enclosure is expected to be nonuniform. Be-

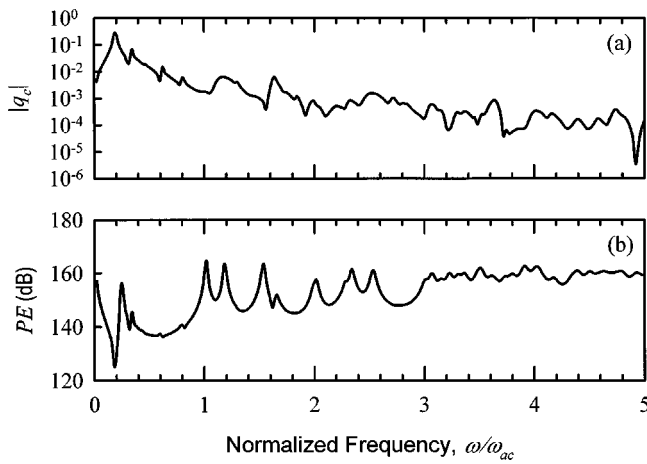


FIG. 11. (a) Secondary source strength of potential energy control for primary acoustic source at $\theta = \pi/6$, $\alpha = \pi/4$ and secondary source at (L_{x1}, L_{x2}, L_{x3}) . (b) Total potential energy of acoustic source strength of unity at (L_{x1}, L_{x2}, L_{x3}) . All data presented are in dB ref 10^{-12} Nm.

sides, the attenuation of sound pressure at all points inside an enclosed space is not necessary from the building services engineer's point of view, as only some portions of an enclosed space will be occupied by people. The creation of appropriate quiet zones is therefore more important. For example, it is desirable to produce quiet zones at noise-sensitive areas inside an enclosure, to reduce the impact of noise on workers in a plantroom. Also, the quiet zone in front of the walls will help to reduce the direct sound transmission. An understanding of the actual sound field under active control of sound transmission, especially at the low frequency range, is required for a detailed description of the effectiveness of the control algorithms.

V. VISUALIZATION OF SOUND ATTENUATION

As mentioned previously, the evaluation of a sound field under active control is of practical importance due to the limitation of the potential energy analysis. The visualization of a sound field inside the enclosure is decisive in the evaluation of the performance of the active control of sound, as it gives an idea of the distributions of the quiet and amplification zones, as well as the degree of their effects in the enclosure. In the present investigation, the numerical model is divided into $21 \times 21 \times 21$ uniform grid points throughout the enclosure, and the attenuation of the sound pressure level (SPL) is found from the difference between the calculated SPL before and after activating the acoustic secondary source by using Eq. (5).

Figure 12(a) shows the SPL attenuation at $\omega = 0.3\omega_{ac}$ inside the enclosure with $\eta_c = 0.01$ and $\varphi = 1.04$ under the potential energy control. It can be observed that a high global reduction of SPL can be achieved at all points inside the enclosure. The peak quiet zone is located between the center of the enclosure and the flexible panel ($x2/L_{x2} = 0$). Such high global reductions of SPL are also found at even lower frequencies. At $\omega = 0.7\omega_{ac}$, amplification zones appear near to the secondary source and on the $x1-x3$ wall on the side of the secondary source as shown in Fig. 12(b), though there is an attenuation of PE at this frequency (Fig. 9). The corre-

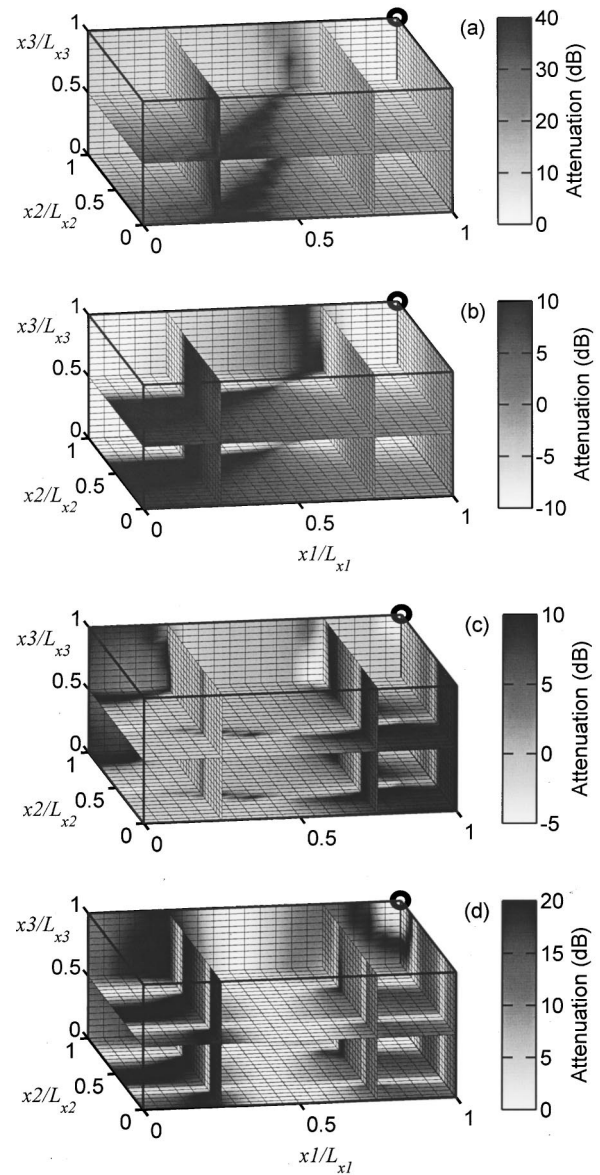


FIG. 12. Attenuation of SPL under potential energy control for primary source at $\theta = \pi/6$, $\alpha = \pi/4$ at different forcing frequencies. (a) $0.3\omega_{ac}$; (b) $0.7\omega_{ac}$; (c) $1.7\omega_{ac}$; (d) $2.5\omega_{ac}$. Secondary source at (L_x, L_y, L_z) ; $\eta_c = 0.01$ and $\varphi = 1.04$.

sponding major quiet zone is found at the corner opposite to the acoustic control source. As the frequency increases beyond $0.7\omega_{ac}$, the quiet zones and the amplification zones are discretely distributed throughout the enclosure. At higher frequencies, the coexistence of quiet and amplification zones is observed, while the total potential energy attenuation is insignificant. An example is shown in Fig. 12(c), where $\omega = 1.7\omega_{ac}$ (cf. Fig. 9). High global control of SPL can also be found at some eigenfrequencies [for instance, at $\omega = 2.5\omega_{ac}$ as shown in Fig. 12(d)], but the quiet zones are observed at discretely confined areas inside the enclosure. Thus, the previous analysis of total potential energy can only effectively indicate the dominance of the quiet zones or the amplification zones. Figures 13(a) and (b) illustrate the sound pressure distributions at $\omega = 1.7\omega_{ac}$ and $2.5\omega_{ac}$ without the active control, respectively. It can be observed that the amplification and the quiet zones under the active control do not col-

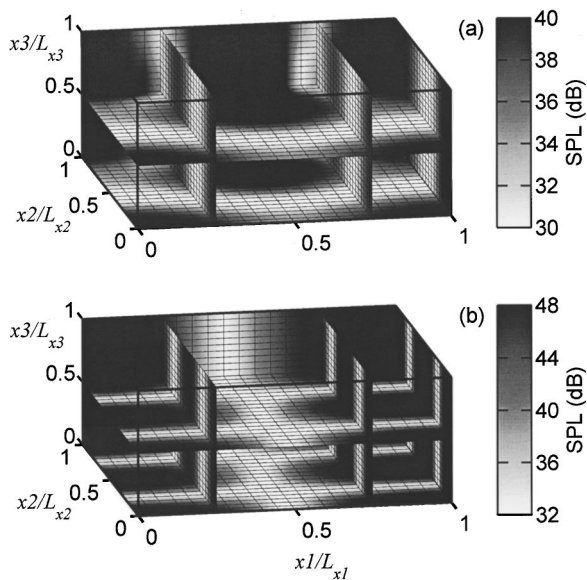


FIG. 13. SPL for primary source at $\theta = \pi/6$, $\alpha = \pi/4$ at different forcing frequencies. (a) $1.7\omega_{ac}$; (b) $2.5\omega_{ac}$. $\eta_c = 0.01$ and $\varphi = 1.04$. All data presented are in dB ref 2×10^{-5} N/m².

lapse with the nodal planes. No nodal plane is observed within the enclosure for $\omega < \omega_{ac}$. The magnitude of the sound field decreases at increased distance from the flexible panel wall.

Detrimental effects appear at some frequencies under the squared pressure control scheme as discussed before. This is due to the destructive interference of acoustic modes at the location of the error sensor.¹⁴ A large increase of SPL throughout the enclosure can also be observed except at the location of the error sensor $(0.9L_{x1}, 0.9L_{x2}, 0.9L_{x3})$, as shown in Fig. 14(a) at $\omega = 0.3\omega_{ac}$ [one of the detrimental effects shown in Fig. 9(a)]. Quiet zones reappear at $\omega = 0.7\omega_{ac}$, as shown in Fig. 14(b). For increasing frequency beyond ω_{ac} , the quiet zones at the position of the error sensor quickly shrink in size, except at some acoustic mode frequencies as mentioned earlier. Detrimental effects are also observed at higher frequencies, resulting in a nearly global amplification [Fig. 14(c)]. In addition, discrete quiet zones and amplification zones occur as frequency increases beyond $2\omega_{ac}$. A typical example is shown in Fig. 14(d), with $\omega = 2.9\omega_{ac}$.

The resultant SPL attenuation maps under the energy density control are similar to those under the squared pressure control, especially under remote error sensing. However, it is observed that the energy density control has the benefit of providing a more uniform SPL attenuation at most frequencies, and avoiding the occurrence of large localized attenuation in the expense of large sound amplifications at other locations. Since there is no significant attenuation produced by the energy density control due to small optimal secondary source strength for the error sensor near to the secondary source at frequency below $0.7\omega_{ac}$, the corresponding sound attenuation patterns are not discussed.

Figure 15 illustrates some examples of the SPL attenuation maps obtained under the energy density control with $\eta_c = 0.01$ and $\varphi = 1.04$. The error sensor is located at

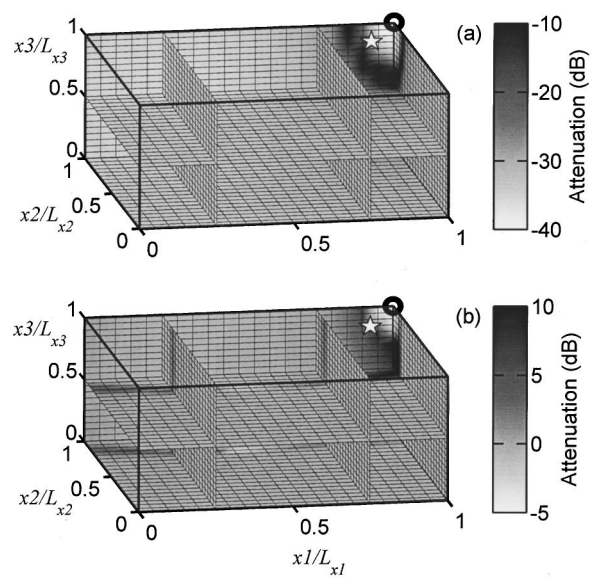


FIG. 14. Attenuation of SPL under squared pressure control for primary source at $\theta = \pi/6$, $\alpha = \pi/4$ at different forcing frequencies. (a) $0.3\omega_{ac}$; (b) $0.7\omega_{ac}$; (c) $1.7\omega_{ac}$; (d) $2.9\omega_{ac}$. Secondary source at (L_x, L_y, L_z) ; error sensor, \star , at $(0.9L_x, 0.9L_y, 0.9L_z)$; $\eta_c = 0.01$ and $\varphi = 1.04$.

$(0.9L_{x1}, 0.9L_{x2}, 0.9L_{x3})$. It can be observed from Fig. 15(a) that the energy density control can provide SPL attenuation globally at $0.7\omega_{ac}$, while both the potential energy and the squared pressure controls produce amplification zones inside the enclosure [Figs. 12(b) and 14(b)]. The energy density control produce much less amplification of PE and SPL inside the enclosure at the frequencies of detrimental effects than the squared pressure control as shown in Fig. 15(b) ($\omega = 1.7\omega_{ac}$). Again the amplification and the quiet zones do not collapse with the SPL nodal planes shown in Fig. 13.

For a stronger cavity-panel coupling system ($\eta_c = 0.26$ and $\varphi = 5.21$), though the attenuation of PE is small at $\omega = 0.2\omega_{ac}$ (Fig. 10), global control of sound field and a quiet zone near to the secondary source under the potential energy control are still achievable as shown in Fig. 16(a). For frequencies below ω_{ac} , except for those near to $0.19\omega_{ac}$, wider quiet zone compared to that in Fig. 12(a) can be ob-

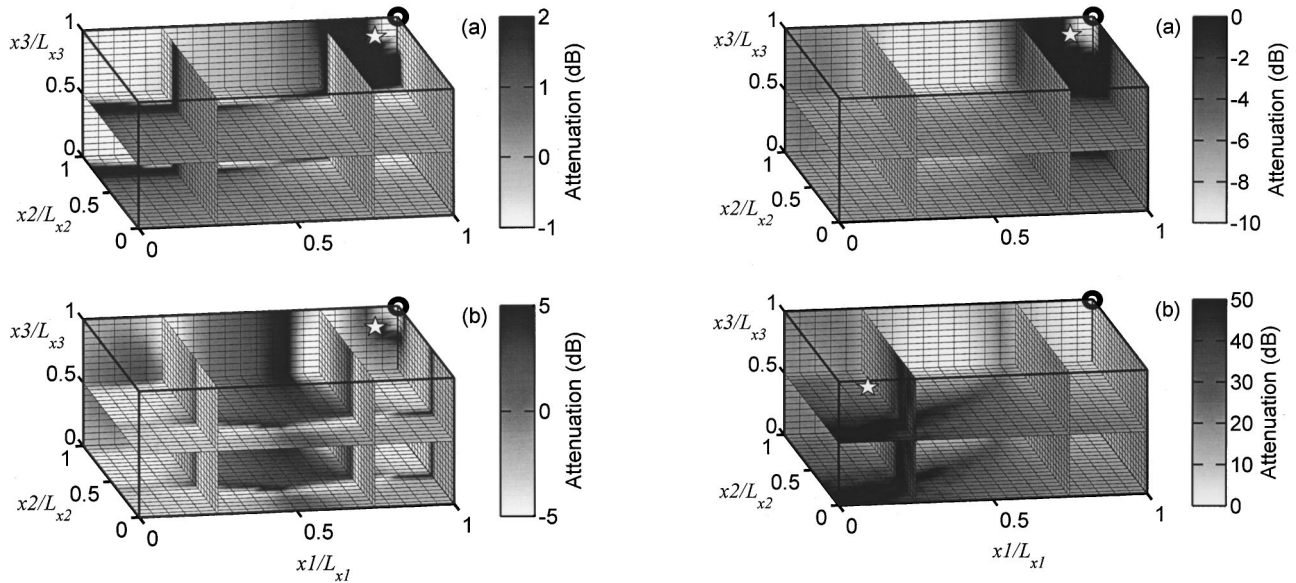


FIG. 15. Attenuation of SPL under energy density control for primary source at $\theta = \pi/6$, $\alpha = \pi/4$ at different forcing frequencies. (a) $0.7\omega_{ac}$; (b) $1.7\omega_{ac}$. Secondary source at (L_x, L_y, L_z) ; error sensor, \star , at $(0.9L_x, 0.9L_y, 0.9L_z)$; $\eta_c = 0.01$ and $\varphi = 1.04$.

served with a stronger structural-acoustic coupled system as shown in Fig. 16(b) ($\omega = 0.3\omega_{ac}$). The sound field pattern is similar to the previous system with $\eta_c = 0.01$ and $\varphi = 1.04$ as frequency increases, especially for $\omega > 2\omega_{ac}$ (not shown here).

Figure 17(a) shows the SPL attenuation under the squared pressure control with near field error sensing at $(0.9L_{x1}, 0.9L_{x2}, 0.9L_{x3})$, with $\eta_c = 0.26$, $\varphi = 5.21$ and $\omega = 0.3\omega_{ac}$ [one of the detrimental effects shown in Fig. 10(a)]. Amplification of SPL can be observed throughout the enclosure, except at the error sensor location, but it is much alleviated [cf. Fig. 14(a)] for the present stronger coupled system. For the remote error sensor at

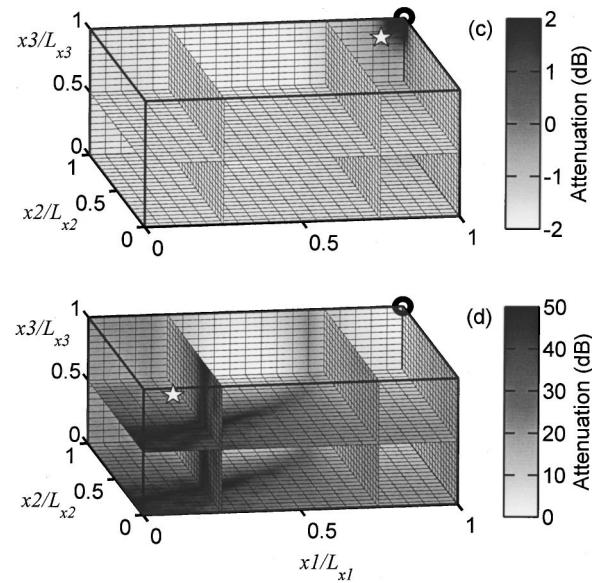


FIG. 17. Attenuation of SPL under squared pressure and energy density control algorithms for primary source at $\theta = \pi/6$, $\alpha = \pi/4$ at $0.3\omega_{ac}$. (a) Squared pressure control, error sensor at $(0.9L_x, 0.9L_y, 0.9L_z)$; (b) squared pressure control, error sensor at $(0.1L_x, 0.1L_y, 0.9L_z)$; (c) energy density control, error sensor at $(0.9L_x, 0.9L_y, 0.9L_z)$; (d) energy density control, error sensor at $(0.1L_x, 0.1L_y, 0.9L_z)$; secondary source at (L_x, L_y, L_z) ; $\eta_c = 0.26$ and $\varphi = 5.21$. \star : error sensor location.

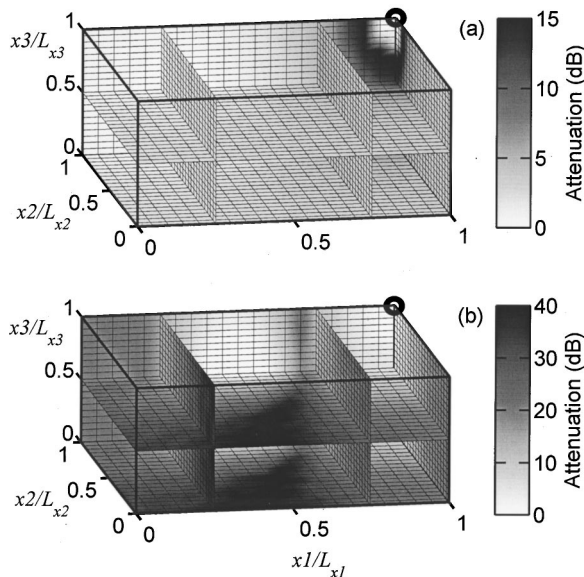


FIG. 16. Attenuation of SPL under potential energy control for primary source at $\theta = \pi/6$, $\alpha = \pi/4$ at different forcing frequencies. (a) $0.2\omega_{ac}$; (b) $0.3\omega_{ac}$. Secondary source at (L_x, L_y, L_z) ; $\eta_c = 0.26$ and $\varphi = 5.21$.

$(0.1L_{x1}, 0.1L_{x2}, 0.9L_{x3})$, higher SPL attenuation can be obtained at $0.3\omega_{ac}$ [as shown in Fig. 17(b)] under the squared pressure control compared with Fig. 17(a). Energy density control eliminates large amplification of sound pressures for near field error sensing at the frequencies of the detrimental effects, as shown in Fig. 17(c). In most cases studied, there is an inherent tendency for the squared pressure control to provide a high level of SPL attenuation at the error sensor locations, at the expense of SPL amplification at other areas, resulting in highly nonuniform noise attenuation, while the energy density control tends to minimize both potential (acoustic pressure) and kinetic (acoustic pressure gradient to a certain extent) energy density at error sensor locations and thus gives a more uniform control of sound field, especially at the frequency of detrimental effects as illustrated in Figs.

17(a) and (c). The resultant sound field under the energy density control with a remote error sensor is similar to that under the squared pressure control. Figure 17(d) gives a typical example of this phenomenon.

Snyder and Hansen²⁴ suggested that the optimum error microphone locations are the points of minimum sound pressure in the optimally controlled residual sound field created by a vibrating panel, while Ruckman and Fuller²⁵ proposed the locations to be at the antinodes of a vibrating cylindrical shell. Their studies evaluated the performance of active control in a free field. However, the problem becomes more complicated when the active sound transmission control inside an enclosure is concerned. Confusion exists between the nodal points and the points of minimum sound pressure under optimum control. In addition, different system performance may be found when the error sensing is done at the antinodes of sound pressure inside an enclosure (for example, see Figs. 9 and 10). Also, both the nodes and antinodes inside the enclosure cannot be easily predicted for frequencies other than the eigenfrequencies. For all the cases investigated in the present study, it is observed that forcing the quiet zone by the squared pressure control with error sensor located at the amplification zones or areas of low SPL attenuation under the potential energy control will increase SPL at other areas adversely. A typical example is shown in Fig. 17(a), where the error sensor is located near to the point of minimum SPL attenuation under the potential energy control [Fig. 16(b)]. In turn, placing the error sensor near to the peak quiet zones of potential energy control results in much better performance of global control effectiveness [Fig. 17(b)]. Though the present finding is obtained in an enclosure, it appears in line with those of free field control.²⁴ Similar results can be obtained for other combinations of θ and α .

In general, the acoustic energy density field is more uniform than the sound field inside the enclosure. Thus, the performance of the energy density control is less dependent on the error sensor locations than the squared pressure control. This has been proved by Parkins *et al.*¹⁸ through an investigation of node structures. However, unsatisfactory energy density control and squared pressure control may still be found in some areas of nonuniform energy density field inside the enclosure, besides the nodal volumes.¹⁴ Figure 18 shows the attenuation of the energy density inside the enclosure under the potential energy control at $0.7\omega_{ac}$ and $1.7\omega_{ac}$ with $\eta_c=0.01$ and $\varphi=1.04$. Large amplification of energy densities at the positions near to the secondary acoustic source can be observed for all cases in the present study, due to the secondary acoustic source.¹⁴ While the energy density fields inside most areas in the enclosure are uniform (Fig. 19), the high energy density at $(0.9L_{x1}, 0.9L_{x2}, 0.9L_{x3})$ lowers the performance of the energy density control as shown previously in Figs. 9(a) and 10(a) if the error sensor is located there. Placing the error sensor, for instance, at $(0.1L_{x1}, 0.1L_{x2}, 0.9L_{x3})$, which is the location of high energy density attenuation under the potential energy control (Fig. 18), produces better PE attenuation [Figs. 9(e) and 10(e)] and sound field control [Fig. 17(d)] under the energy density error sensing scheme.

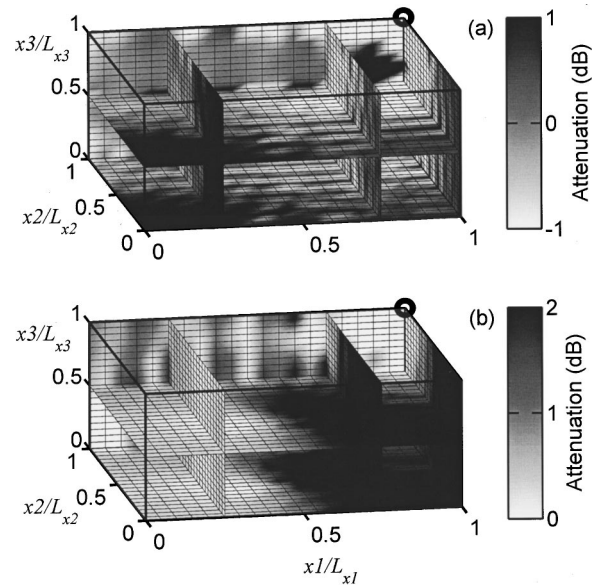


FIG. 18. Attenuation of energy density under potential energy control for primary source at $\theta=\pi/6$, $\alpha=\pi/4$ at different forcing frequencies. (a) $0.7\omega_{ac}$; (b) $1.7\omega_{ac}$. Secondary source at (L_x, L_y, L_z) ; $\eta_c=0.01$ and $\varphi=1.04$.

VI. CONCLUSIONS

This study investigates the effectiveness of active control of sound transmission into a slightly damped rectangular enclosed space. The performance of three different control algorithms, namely the potential energy control, the squared pressure control, and the energy density control, are investigated and compared in terms of the overall potential energy attenuation and the resultant sound pressure level attenuation patterns. A compact matrix formulation of the analytical steady-state solution under the energy density control is derived based on the application of the impedance-mobility

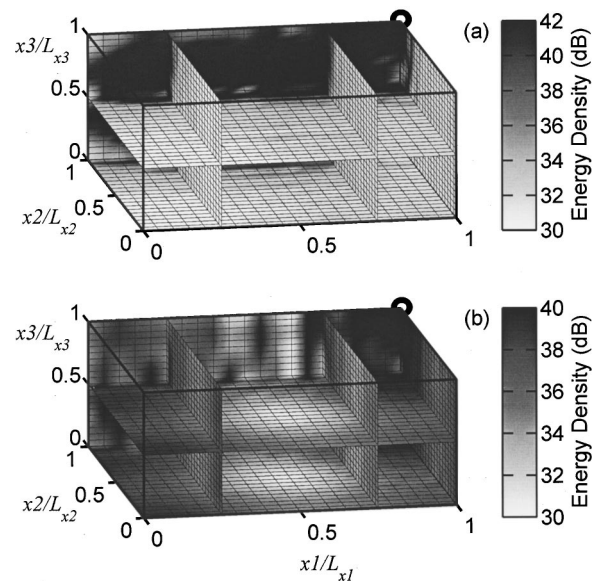


FIG. 19. Energy density under potential energy control for primary source at $\theta=\pi/6$, $\alpha=\pi/4$ at different forcing frequencies. (a) $0.7\omega_{ac}$; (b) $1.7\omega_{ac}$. Secondary source at (L_x, L_y, L_z) ; $\eta_c=0.01$ and $\varphi=1.04$. All data presented are in dB ref 10^{-12} N/m².

approach to a fully structural-acoustic coupled system. The frequency range in the present study extends to five times the first eigenfrequency of the enclosure.

Two control categories are classified in the potential energy analysis. One is for the case where the first eigenfrequency of the acoustic (cavity) mode is less than that of the structural (panel) mode, while the other is the opposite. For both categories, high potential energy attenuation under potential energy control can be achieved for driving frequency below the first resonance frequency of the structural mode, while for the latter, acoustic control source is also effective at the frequency beyond this structural mode frequency, but is ineffective at this frequency. Active vibration control is shown to be ineffective in the cavity-controlled modes.

It is shown that both quiet zones and amplification zones are created under all the control algorithms investigated, except at frequencies far below the first eigenfrequency of the cavity. High global reduction of the sound level can also be obtained at some acoustic eigenfrequencies under the potential energy control, but the quiet zones are discrete. In general, the potential energy control gives the best performance among the control algorithms studied, but it is difficult to implement.

Detrimental effects have been observed under the squared pressure control of sound transmission due to the inherent destructive modal interference at the position of the error sensor. At the frequencies of the detrimental effects, extremely localized sound attenuation with global amplification of the sound level is found. This adverse effect can be alleviated by remote error sensing or by applying the energy density control. The energy density control has the advantage of fewer detrimental effects than squared pressure control. It is ineffective for near field sensing due to nonuniform energy density near to the secondary source. However, the energy density control can eliminate the disadvantages of both detrimental effects and spillovers, and can provide a more uniform attenuation of sound pressures. For remote error sensing strategy, the squared pressure and the energy density controls give similar resultant sound fields.

Sound and energy density fields under the potential energy control give the preferential error sensor locations for the creation of quiet zones under the squared pressure and energy density controls, which cannot be found from the potential energy analysis of previous studies. Forcing the quiet zones of the squared pressure and energy density controls at the amplification zones of the potential energy control has adverse effects on the sound attenuation, resulting in ineffective active sound transmission control. Also, maximum performance of active control can be found when the error sensor is located at the peak quiet zones and peak energy density attenuation zones under the potential energy control for the squared pressure and the energy density controls respectively.

To conclude, the results obtained in the present study address some issues which, to the knowledge of the authors, are not fully addressed by the existing literature. They show clearly the inadequacy of the use of the total potential acoustic energy as a measure of three-dimensional active sound transmission control performance, especially when the driv-

ing frequency is higher than the first eigenfrequency of the enclosure. Large global increase of sound field is observed when localized quiet zones are improperly forced. This can hardly be indicated in the traditional potential energy attenuation plots. This paper also suggests an analysis of the global and local effectiveness of active sound transmission control using visualization of the sound field in conjunction with the total acoustic potential energy attenuation. Besides, it is shown that the optimal error sensor locations for the squared pressure and energy density controls can then be found from the resultant sound fields and energy density fields under the potential energy control scheme, respectively. Moreover, it is illustrated that the acoustic control source is worthwhile for practical use, especially for active sound transmission control. Finally, it is found that in general, for stronger structural-acoustic coupling systems, wider quiet zones and alleviated detrimental effects can be found compared with the weak structural-acoustic coupling systems. A more detailed investigation concerning the effects of the strength of structural-acoustic coupling on the performance of active control would be worthwhile.

ACKNOWLEDGMENTS

The financial support of the Hong Kong Polytechnic University and the Research Grant Council, HKSAR Government is gratefully acknowledged.

- ¹P. Scuri, *Design of Enclosed Spaces* (Chapman and Hall, New York, 1995).
- ²C. R. Fuller and J. D. Jones, "Experiments on reduction of propeller induced interior noise by active control of cylinder vibration," *J. Sound Vib.* **112**, 389–395 (1987).
- ³J. Pan, C. H. Hansen, and D. A. Bies, "Active control of noise transmission through a panel into a cavity: I. Analytical study," *J. Acoust. Soc. Am.* **87**, 2098–2108 (1990).
- ⁴J. Pan and C. H. Hansen, "Active control of noise transmission through a panel into a cavity: II. Experimental study," *J. Acoust. Soc. Am.* **90**, 1488–1492 (1991).
- ⁵J. Pan and C. H. Hansen, "Active control of noise transmission through a panel into a cavity: III. Effect of the actuator location," *J. Acoust. Soc. Am.* **90**, 1493–1501 (1991).
- ⁶X. J. Qiu, J. Z. Sha, and J. Yang, "Mechanisms of active control of noise transmission through a panel into a cavity using a point force actuator on the panel," *J. Sound Vib.* **182**, 167–170 (1995).
- ⁷B. S. Cazzolato and C. H. Hansen, "Active control of sound transmission using structural error sensing," *J. Acoust. Soc. Am.* **104**, 2878–2889 (1998).
- ⁸S. D. Snyder and C. H. Hansen, "The design of systems to control actively periodic sound transmission into enclosed spaces, part I: Analytical models," *J. Sound Vib.* **170**, 433–449 (1994).
- ⁹S. D. Snyder and C. H. Hansen, "The design of systems to control actively periodic sound transmission into enclosed space, part II: Mechanisms and trends," *J. Sound Vib.* **170**, 451–472 (1994).
- ¹⁰S. M. Kim and M. J. Brennan, "A comparative study of feedforward control of harmonic and random sound transmission into an acoustic enclosure," *J. Sound Vib.* **226**, 549–571 (1999).
- ¹¹P. Joseph, S. J. Elliott, and P. A. Nelson, "Near field zones of quiet," *J. Sound Vib.* **172**, 605–627 (1994).
- ¹²S. D. Sommerfeldt and P. J. Nashif, "An adaptive filtered-x algorithm for energy-based active control," *J. Acoust. Soc. Am.* **96**, 300–306 (1994).
- ¹³Y. C. Park and S. D. Sommerfeldt, "Global attenuation of broadband noise fields using energy density control," *J. Acoust. Soc. Am.* **101**, 350–359 (1997).
- ¹⁴S. K. Lau and S. K. Tang, "Sound fields in a slightly damped rectangular enclosure under active control," *J. Sound Vib.* **238**, 637–660 (2000).
- ¹⁵A. Sampath and B. Balachandran, "Studies on performance functions for interior noise control," *Smart Mater. Struct.* **6**, 315–332 (1997).

- ¹⁶B. S. Cazzolato, "Sensing systems for active control of sound transmission into cavities," Ph.D. thesis, The University of Adelaide, Australia, 1999.
- ¹⁷S. M. Kim, "Active control of sound in structural-acoustic coupled systems," Ph.D. thesis, University of Southampton, United Kingdom, 1998.
- ¹⁸J. W. Parkins, J. Tichy, and S. D. Sommerfeldt, "A comparison of two active control methods through an investigation of node structures," *Proc. ACTIVE 99* **2**, 729–740 (1999).
- ¹⁹P. Joseph, S. J. Elliott, and P. A. Nelson, "Statistical aspects of active control in harmonic enclosed sound fields," *J. Sound Vib.* **172**, 629–655 (1994).
- ²⁰P. A. Nelson and S. J. Elliott, *Active Control of Sound* (Academic, London, 1992).
- ²¹D. Roylance, *Mechanics of Materials* (Wiley, New York, 1996).
- ²²S. M. Kim and M. J. Brennan, "A compact matrix formulation using the impedance and mobility approach for the analysis of structural-acoustic system," *J. Sound Vib.* **223**, 97–113 (1999).
- ²³A. J. Bullmore, P. A. Nelson, A. R. D. Curtis, and S. J. Elliott, "The active minimization of harmonic enclosed sound field, part II: computer simulation," *J. Sound Vib.* **117**, 15–33 (1987).
- ²⁴S. D. Snyder and C. H. Hansen, "Using multiple regression to optimize active noise control system design," *J. Sound Vib.* **148**, 537–542 (1991).
- ²⁵C. E. Ruckman and C. R. Fuller, "Optimizing actuator locations in active noise control systems using subset selection," *J. Sound Vib.* **186**, 395–406 (1995).